Accepted Manuscript

On the nature of the room temperature ferromagnetism in nanoparticulate co-doped ZnO thin films prepared by EB-PVD

Niko Churata Mamani, Rafael Tomaz da Silva, Angela Ortiz de Zevallos, Alexandre Alberto Chaves Cotta, Waldemar Augusto de Almeida Macedo, Máximo Siu Li, Maria Inês Basso Bernardi, Antonio Carlos Doriguetto, Hugo Bonette de Carvalho

PII: S0925-8388(16)33663-5

DOI: 10.1016/j.jallcom.2016.11.183

Reference: JALCOM 39680

To appear in: *Journal of Alloys and Compounds*

Received Date: 16 September 2016

Revised Date: 10 November 2016

Accepted Date: 13 November 2016

Please cite this article as: N.C. Mamani, R.T. da Silva, A.O. de Zevallos, A.A. Chaves Cotta, W.A. de Almeida Macedo, M.S. Li, M.I.B. Bernardi, A.C. Doriguetto, H.B. de Carvalho, On the nature of the room temperature ferromagnetism in nanoparticulate co-doped ZnO thin films prepared by EB-PVD, *Journal of Alloys and Compounds* (2016), doi: 10.1016/j.jallcom.2016.11.183.

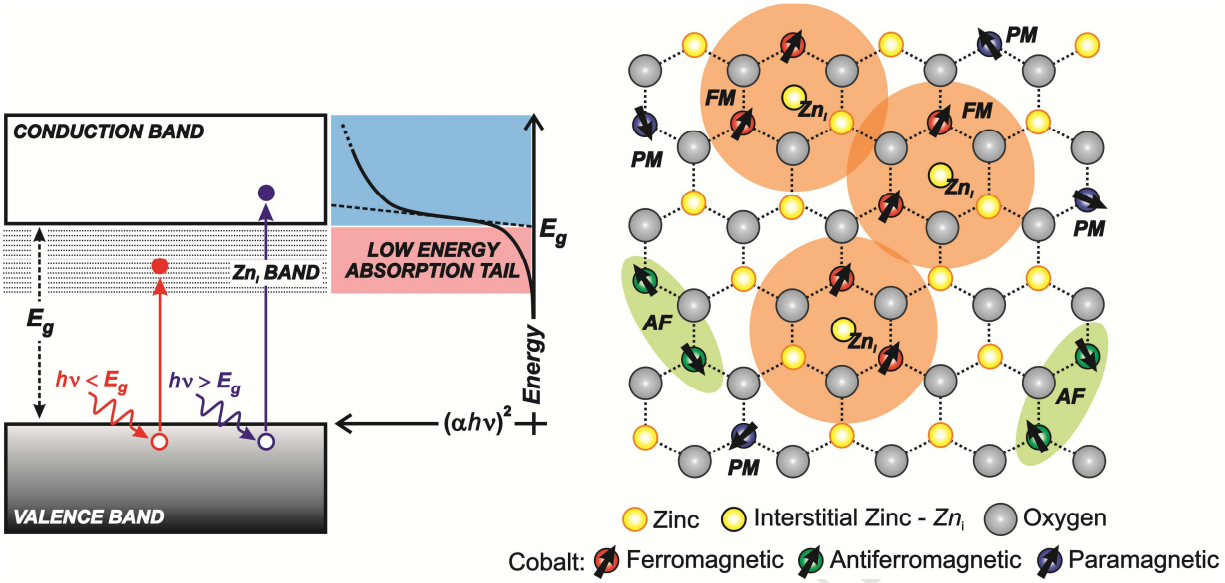

On the nature of the room temperature ferromagnetism in nanoparticulate Co-doped ZnO thin films prepared by EB-PVD

Niko Churata Mamani,[a] *Rafael Tomaz da Silva,*[a] *Angela Ortiz de Zevallos,*[a] *Alexandre Alberto Chaves Cotta,*[b,c] *Waldemar Augusto de Almeida Macedo,*[b] *Máximo Siu Li,*[d] *Maria Inês Basso Bernardi,*[d] *Antonio Carlos Doriguetto,*[a] *Hugo Bonette de Carvalho*[a]*

[a] Universidade Federal de Alfenas, 37130-000 Alfenas, MG, Brazil.

[b] Centro de Desenvolvimento da Tecnologia Nuclear, CDTN, 31270-901 Belo Horizonte, MG, Brazil.

[c] Departamento de Física, Universidade Federal de Lavras, 37200-000 Lavras, MG, Brazil.

[d] Instituto de Física de São Carlos, USP – Universidade de São Paulo, 13560-970 São Carlos, SP, Brazil

ABSTRACT: The complete comprehension of the magnetic properties of the dilute magnetic oxides has emerged as one of the major challenges in the fields of materials science and condensed matter physics. Up to now, there is no consensus about the mechanism behind the so often observed room temperature ferromagnetism. However it is well known that defects plays an important role in the context. Here we present the study of the correlation between the structural and the magnetic properties of nanoparticulate Co-doped ZnO ($Zn_{1-x}Co_xO$, x = 0.02 and 0.08) thin films prepared via Electron Beam-Physical Vapor Deposition. The structural results confirms the incorporation of the Co^{2+} ions into the ZnO host matrix with no secondary phases. Magnetic measurements show a robust ferromagnetic order for the thin film with x = 0.08, whereas for the sample with x = 0.02 only a tiny ferromagnetism were observed. We could explain the differences in the magnetic behaviour entirely under the scope of the the spin-split impurity band model. In this work we also present convincing

evidences of the no correlation between the oxygen vacancies and the desired room temperature ferromagnetism.

1. INTRODUCTION

The development of spintronic devices based on metallic systems is undoubtedly a successful research area [1-3]. Besides, interesting theoretical and experimental properties have been reported on metal/semiconductor hybrid systems [4, 5]. However, the initial and direct applicability of such systems was hindered by the low spin injection efficiency due to the well know impedance mismatch across the interface between both materials [6]. This problem was further overcome by using either ballistic electrons [7] or very thin tunnelling barriers between the ferromagnet and the semiconductor [8, 9]. Besides, another approach to solve the spin-injection problem would be the use of ferromagnetic semiconductors instead of magnetic metals. Particularly, a new class of materials called dilute magnetic semiconductors (DMS) are attracting intense interest. Mn-doped III-V semiconductors were found to be ferromagnetic, introducing very special new properties, like the electrical control of the magnetization and the Curie temperature (T_C) [10]. Nevertheless, the T_C for these materials is still far below room temperature, not exceeding 200 K [11, 12].

In this context, the study of the magnetic properties of transition metal (TM) doped large band gap semiconductors was triggered by the theoretical work of Dietl *et al.* reporting a room temperature ferromagnetism (RTFM) for the Mn-doped GaN and ZnO [13]. After all, a huge effort has been concentrated on TM-doped oxides, the dilute magnetic oxides (DMOs), as ZnO, TiO_2 and SnO_2 [14-16]. However, in spite of the extensive investigations, the origin of the observed RTFM for the DMOs remains inconclusive and controversial. Up to now, the consensus is that defects play an important role to drive the ferromagnetic behavior [17, 18], which could explain the disparity among experimental reports and the attested high sensibility to the preparation conditions observed for the DMOs [19].

From the theoretical point of view, in the literature one can find several different models to explain

the usual observed RTFM. Early works on such systems attributed the ferromagnetic order to a carrier-mediated mechanism based on the Zener model [13]. However, it could not account for the RTFM in insulating systems. For those cases Coey *et al*. proposed in 2005 the spin-split impurity band model, also called bound magnetic polaron (BMP) theory [20]. The main common feature of these models is the importance of an exchange interaction between the charge carriers introduced in the oxide host through specific point defects and the magnetic dopants. It is also important to mention a sub-category of BMP theory named F-center exchange (FCE) [21] and the charge-transfer ferromagnetism (CTF) [22]. By your turn, the CTF model were introduced to account for more specific unexplained experimental observations, like moments exceeding the maximum possible spin moment per cation [23]. In contrast to the other models, the magnetic moments in the CTF are entirely localized on itinerant carriers confined in small regions, such as grain boundaries and interfaces [22]. In the same direction, Straumal *et al.* have also proposed another model relating the RTFM in nanoparticulate doped and undoped oxides [24, 25] to magnetic moments of unpaired electrons residing in specific electronic states at the grain boundaries of the nanoparticles. There, they have established an empirical grain size threshold value of around 33 nm below what the ferromagnetism would occur [24].

In this work we present a study concerning the preparation of nanoparticulate Co-doped ZnO thin films via Electron Beam-Physical Vapor Deposition (EB-PVD), and the correlation between their structures and magnetic properties. Here we demonstrated that the RTFM can be entirely associated to the BMP model connected to the presence of a shallow-donor zinc interstitial (Zn_i) defect band.

2. EXPERIMENTAL

Nanoparticulate Co-doped ZnO ($Zn_{1-x}Co_xO$) thin films with Co concentration of x = 0.02 and 0.08 were prepared via EB-PVD on glass substrates. Ceramic targets were prepared via standard solid-state reaction method following the procedures described in Ref. [26] with Co content of x = 0.04 and 0.16

for the thin films with x = 0.02 and 0.08, respectively. The details concerning the deposition system can be found in Ref. [27]. The deposition was carried out at room temperature in an evaporation chamber using an electron beam gun (Telemark-231) operating at 3.6 kV with beam current of 20 mA in high vacuum (4×10^{-6} Torr). The controlling of the thickness of the sample was performed through the time of evaporation after a calibration procedure. The deposition rates were 25 Å/s for the film with x = 0.02 and 8 Å/s for the film with x = 0.08. The difference in the rates correspond to different resistivities of the ceramic targets on the Co content [23, 28]. After deposition the thin films were annealed at 400 ^{o}C, heating/cooling rate of 10 °C/min., in air atmosphere for 2 hours in order to increase crystallinity. The thickness of the thin films were measured using a Talystep Taylor–Hobson profiler. The measured thickness for both thin films were of the order of 500 nm.

The structural properties of the thin films were investigated by X-ray diffraction (XRD) performed in the range of 2θ = 20°−80° in steps of 0.02° at 5 s/step using CuKα radiation (λ = 1.542 Å) and a graphite monochromator in a Rigaku Ultima IV diffractometer. Raman spectroscopy was used to study the incorporation of dopants and the resulting lattice disorder of the host lattice. Raman measurements was carried out at room temperature in the backscattering geometry using an excitation soli-state laser at 532 nm. We used an optical lens with 100× magnification, which supplies an average laser spot size of 1 μm. In order to increase the statistics of the measurements, several spectra were recorded at different points randomly chosen over the surfaces of the films. The surface structure and chemical composition of the thin films were characterized by scanning electron microscopy (SEM) and energy dispersive X-ray spectroscopy (EDS), respectively. The SEM images and the chemical analyzes were taken using a FEI Inspect F50 high-resolution SEM equipped with Apollo X SDD EDAX EDS probe. UV-VIS measurements were used to evaluate the crystal environment were the Co dopant ions are located in the ZnO host matrix. The UV-VIS spectra of the thin films were collected in transmittance mode in a Cary-17 spectrophotometer, in the region of 200–800 nm. The oxidation state of the dopants

were determined through X-ray photoelectron spectroscopy (XPS) measurements carried out in an ultrahigh vacuum chamber (base pressure better than 2.0 x 10^{-9} mbar) using a monochromatic Al Kα X-ray source with the output power set at 400 W and a SPECS hemispherical electron energy analyzer PHOIBOS 150 MCD. Normal emission scans with 50 eV pass energy for the survey and high-resolution spectra were acquired using a 0.3 μA flood gun emission current for a charge compensation. The CasaXPS was used to analyze all XPS data. Magnetization curves at room temperature were measured using a vibrating-sample magnetometer (VSM) Lakeshore 7404 with a maximum field of 8 kOe.

3. RESULTS AND DISCUSSION

Fig. 1(a) presents the XRD patterns for the nanoparticulate Co-doped ZnO thin films. The observed peaks correspond to those expected for polycrystalline hexagonal wurtzite ZnO, space group $P6_3mc$ (JCPDS 36-1451). No metallic Co or other foreign peaks were observed for both samples within the XRD detection limit, representing a first indication of the Co incorporation into the ZnO matrix in our thin films.

Raman spectra from our set of thin films are shown in Fig. 1(b). The frequency of wurtzite ZnO vibrational modes are well established in the literature [29-31]. Here, we observe two main modes centered at around 380 and 437 cm^{-1} that are assigned to A_1(TO) and E_{2H}, respectively. This result corroborates the obtained DRX data presented in Fig. 1, confirming the ZnO wurtzite structure of the thin films. We also observe a broad band at 500–600 cm^{-1}, which enclose two main vibrational modes centered at ~530 and ~573 cm^{-1}.The latter can be attributed to the overlap of the LO phonons of the A_1 and E_1 and the former to the density of states correspondent to the $2A_1$(LA) in the *M–K* direction of the BZ [29, 32]. This broad band were also observed with different dopant and it is also often attributed to structural intrinsic defects [33-38]. Generally, in pure ZnO samples the A_1(LO) and E_1(LO) modes are

less intense due to destructive interference between the potential deformation and Fröhlich interaction [39]. However, the crystalline disorder induced by the incorporation of dopants, impurities, and defects can amplify these modes due to the consequential break out of the *k*-conservation law, giving rise to a broad band that reflects the density of phonon states around those frequencies [26, 40]. In that sense, the overall observed Raman results also indicate the incorporation of Co into the ZnO matrix in our thin films.

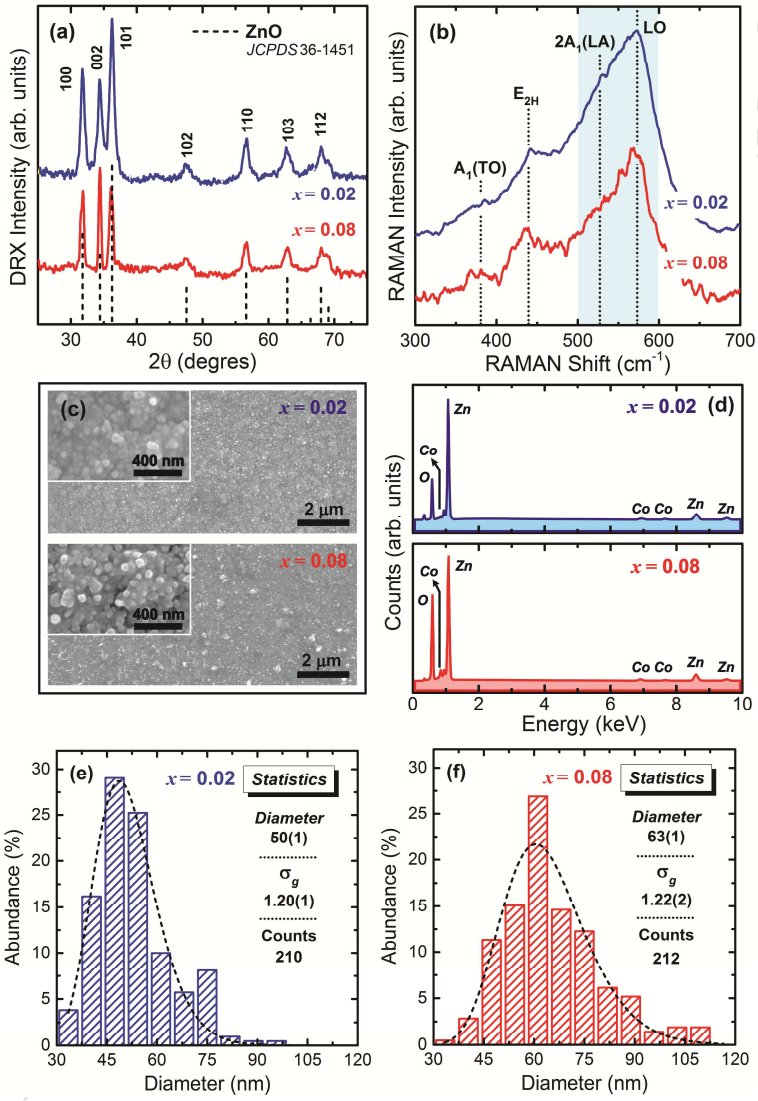

Fig. 1. (a) XRD patterns (CuKα) and (b) Raman spectra for the nanoparticulate Co-doped ZnO thin films. (c) Representative SEM micrographs and (d) EDS spectra of the samples. The inset in (c) revels the nanosized granular pattern of the films. Diameter size distribution histograms for the thin film with (e) $x = 0.02$ and (f) $x = 0.08$ is given. The dashed line in panel (e) and (f) is the log-normal fit.

The morphology of our Co-doped ZnO thin films and their chemical composition were also analyzed by SEM (Fig. 1(c)) and EDS (Fig. 1(d)) measurements, respectively. The images reveal nanoparticulate surfaces (inset of Fig. 1(c)). A statistical analyzes of the particle size distributions gives a geometric average diameter of 50 ± 1 and 60 ± 1 nm, with a standard deviation (σ_g) of 1.20 ± 0.01 and 1.22 ± 0.02, for the thin films with x = 0.02 and x = 0.08, respectively (statistics on Fig. 2(e) and 2(f)). The obtained values for the standard deviation show a narrow size distribution quite close to the condition usually accepted as a monodisperse distribution (σ_g < 1.25) [41]. Images were also acquired using a backscattered electron detector (BSE) in order to highlight any cobalt secondary or segregated phase over the samples surfaces. A series of full scans over large areas show no evidence of Co-rich clusters, strongly suggesting that the Co ions in the studied thin films are in the substitutional character into the Zn sites of the ZnO wurtzite structure. The EDS analyzes were performed in multiple points and also over large areas. The average measured effective Co concentration (x_E) was 0.020 ± 0.004 and 0.078 ± 0.002 for the thin films with x = 0.02 and x = 0.08, respectively.

Fig. 2(a) and 2(b) show the optical transmittance spectra of the Co doped ZnO thin films in the wavelength from 200 to 800 nm (6.20 to 1.55 eV) at room temperature. The observed spectra are quite similar to those previously reported in the literature [42], with the ZnO exciton absorption at around of 380 nm and the Co^{2+} absorption between 500 and 700 nm. The absorption bands observed at approximately 560 (572), 613 (608) and 656 (655) nm for the sample with x = 0.02 (x = 0.08) are attributed to d–d transitions of high spin states of Co^{+2} ions in the tetrahedral sites of the ZnO wurtzite matrix [43]. The Co^{+2} cation is in $3d^7$ configuration with ^4F state corresponding to the lower energy level and the ^4P, ^2G, ^2F, ^2D and ^2P states at higher energies [44]. Once the Co^{+2} cation is sited in a tetrahedral field the ^4F state splits into $^4A_2(F)$, $^4T_2(F)$ and $^4T_1(F)$. Here, the $^4A_2(F)$ correspond to the ground state. The first excited state ^4P does not split, but it is transformed into $^4T_1(P)$. Similarly, ^2G splits into $^2A_1$(G), $^2E(G)$, $^2T_1(G)$ and $^2T_2(G)$. In such scenario the observed absorption peaks at 560

(572), 613 (608) and 656 (655) nm are ascribed to the transitions $^4A_2(F) \rightarrow {}^2A_1(G)$, $^4A_2(F) \rightarrow {}^4T_1(P)$ and $^4A_2(F) \rightarrow {}^2E(G)$, respectively [43]. These transitions in the transmission spectra of our Co-doped ZnO thin films clearly confirms that the Co ions are sited in the Zn sites of the wurtzite ZnO matrix with +2 oxidation state, supporting the previous results from the structural characterization as well.

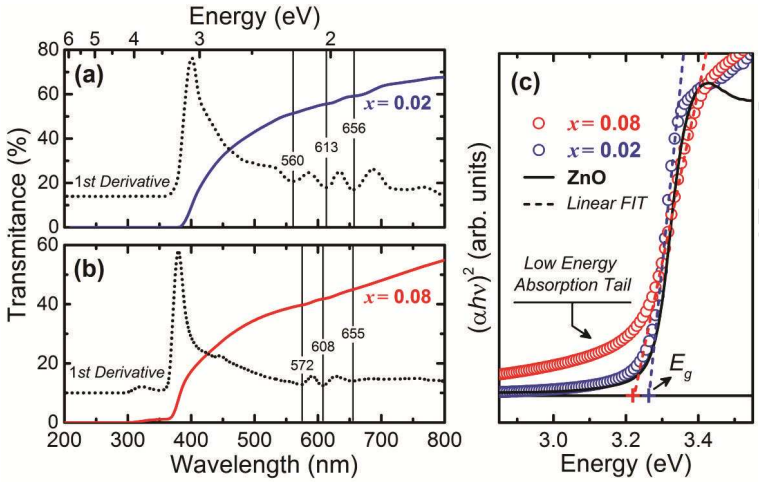

Fig. 2. UV-VIS transmission for the nanoparticulate Co-doped ZnO thin films (a) x = 0.02 and (b) x = 0.08. The dotted lines, corresponding to the first derivative of the transmittance curve, highlight the Co^{2+} absorption bands. (c) Tauc plots of the transmittance spectra. The dashed lines correspond to linear fits of the absorption edges extrapolated to $h\nu = 0$ in order to find E_g. The solid line correspond to the Tauc plot for a reference undoped ZnO thin film.

We also observe in Fig. 2(a) and 2(b) that the transparency of the thin film with x = 0.02 is higher than that for the film with x = 0.08. This can be attributed to differences in the film thickness, which it is estimated in 10% between them. The energy gap (E_g) of the thin films was calculated from the transmittance spectra by Tauc plots (Fig. 2(c)); the obtained values were quite similar to each other, 3.27 ± 0.04 and 3.23 ± 0.03 eV for the films with x = 0.02 and x = 0.08, respectively. Fig. 2(c) also presents a Tauc plot for a reference undoped ZnO thin film prepared at the same condition of the doped ones. The exciton peak is clearly visible in the undoped ZnO thin film indicating a good crystallinity quality. The obtained E_g for the undoped ZnO thin film is 3.28 ± 0.03. These data lead us to conclude that there is no influence of Co-doping over the E_g, since there is no significant changes in

the obtained values. In fact, a Co^{2+} insertion into the ZnO matrix at the Zn^{2+} sites would not expected to lead to significant structural changes, since the tetracoordinated Co^{2+} cation has a crystal radius of 0.72 Å, a value very close to the crystal radius of the tetracoordinated Zn^{2+} in the ZnO wurtzite structure, 0.74 Å [45]. Therefore, the observed invariance of the E_g as a function of the dopant concentration is an additional indication of the substitutional character of the Co-doping in our thin films. It is also important to point out to an absorption tail at lower energies highly evident for the thin film with x = 0.08, as compared with the others ones (Fig. 2(c)). The onset of the absorption tail is around 2.85 eV, and its presence indicates an impurity band near to the conduction band edge due to the overlapping of states introduced by the Co-doping.

The structural properties of the studied thin films were also investigated by XPS. Fig. 3(a) shows the obtained XPS spectrum at the Co 2*p* binding energy. It is observed four peaks corresponding to the $2p_{3/2}$ and $2p_{1/2}$ doublet and the shake up resonance transitions (satellites) of these two peaks at higher binding energies. The energy for the $2p_{3/2}$ and $2p_{1/2}$ doublet obtained by a Gaussian fit of the spectra was 781.4 and 797.1 eV, respectively. The shake-up structure and the energy separation between the $2p_{3/2}$ and $2p_{1/2}$ peaks of $\Delta \approx 15.7$ eV are consistent with the binding energies reported for Co^{2+} ions [46]. The binding energy and the spin-orbit splitting of the Co^0 would be observed at little lower energies, at 778.3 and 793.3 eV ($\Delta \approx 15.0$ eV) [47]. Once the structural results excludes the possibility of cobalt oxide phases in the thin films, the XPS data indicate that a substantial portion of the cobalt ions have a 2+ oxidation state in the Zn sites of the wurtzite ZnO host matrix.

The Zn $2p_{3/2}$ XPS spectra for our thin films are displayed in Fig. 3(b). All the spectra show symmetric single peaks at around 1021.7 eV, a binding energy correspondent to those reported for pure ZnO [46]. The symmetric single peaks rule out the possibility of multiple components of Zn in these samples. No change in the Zn $2p_{3/2}$ peak positions is observed with the increasing of the Co doping, from x = 0.02 to x = 0.08, indicating that Zn ions retain the 2+ oxidation state in both thin

films. However, we note that the intensity of the Zn $2p_{3/2}$ peak decreases as the Co content increases, which indicates that the Co^{2+} cations are incorporating at the Zn sites.

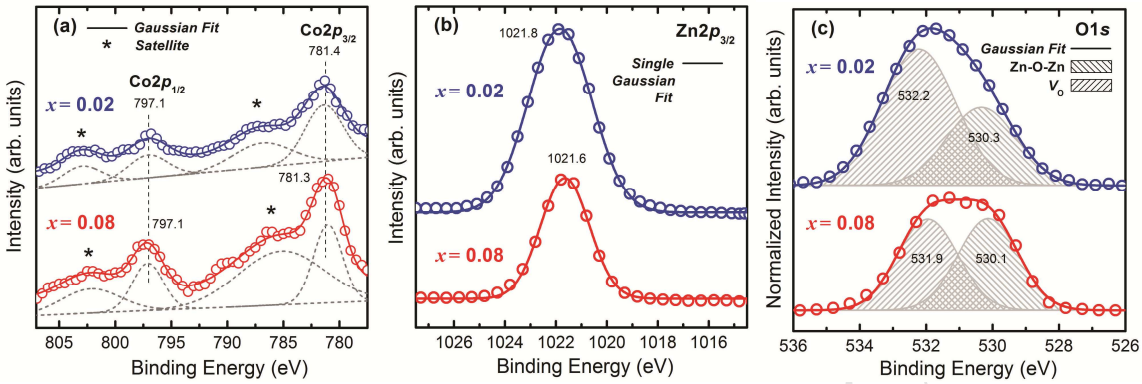

Fig. 3. XPS spectra for the nanoparticulate Co-doped ZnO thin films at binding energies of: (a) Cobalt 2*p*, (b) Zinc $2p_{3/2}$ and (c) Oxygen 1*s* core levels. At (c) the spectra are normalized by the integrated area of the low binding energy component at ~530 eV.

We have also used XPS to probe the density of oxygen vacancies (V_O) in our nanoparticulate Co-doped ZnO thin films. Fig. 3(c) presents the O 1*s* spectra for our set of samples. The O 1*s* peaks exhibit an asymmetry, meaning that more than one kind of oxygen species exists in the thin films. The O 1*s* XPS spectra were fitted by two Gaussian peaks centering at ~530 and ~532 eV and normalized by the integrated area of the peak at ~530 eV. The peak at ~530 eV is attributed to lattice oxygen ions (O^{2-}) in wurtzite ZnO structure [48]. Besides, it has been proved that the high energy binding component at ~532 eV can be ascribed to O^{2-} ions in oxygen-deficient regions (V_O) [49-51]. As can be clearly seen in Fig. 3(c), the intensity of the peak related to the V_O is higher for the thin film with x = 0.02. Therefore, the relatively large contribution of the peak related to V_O for the thin film with x = 0.02 strongly suggests that the density of the V_O is higher for this sample.

In summary, the structural analyzis confirms that the Co^{2+} ions occupy the Zn-sites of the ZnO wurtzite structure in the studied thin films, excluding the presence of any magnetic extrinsic sources, such as Co-rich nanocrystals or segregated secondary magnetic phases. The results also clearly point

that the density of V_O is higher for the thin film with x = 0.02 than for the thin film with x = 0.08. With these considerations, we proceed to magnetic characterization.

The magnetic measurements were performed at room temperature in a vibrating-sample magnetometer (VSM) under magnetic fields up to 8 kOe. The measurements of the magnetic moment (M) as a function of magnetic field (H) are presented in Fig. 4(a). The $M(H)$ reveals the coexistence of a paramagnetic and a ferromagnetic phase for the thin films, as we would expect. For the thin film with x = 0.02 the paramagnetic phase is large as compared to the ferromagnetic phase, the lower-right inset in Fig. 4 highlights the hysteresis corresponding to this phase. On the contrary, for the thin film with x = 0.08 the ferromagnetic component is dominant, the upper-left inset in Fig. 4 highlights, in the range of H above saturation of the ferromagnetic phase, the linear increasing of M correspondent to the relative small paramagnetic phase.

To quantify the magnetic parameters of the coexisting two phases, we used the following expression for M as a function of H [23]:

$$M(H) = \frac{2M_S}{\pi}\tan^{-1}\left[\frac{H \pm H_C}{H_C}\tan\left(\frac{\pi M_R}{2M_S}\right)\right] + \chi_P H\,, \qquad (1)$$

where the first term corresponds to a ferromagnetic hysteresis curve with the saturation magnetization M_S, the remanence M_R and the coercive field H_C. The second term is related to the corresponding paramagnetic susceptibility χ_P. The obtained fitting parameter for both thin films are listed in Table 1.

Table 1. Parameters of the magnetic characterization: effective cobalt concertation (x_E), saturation magnetization (M_S), coercive field (H_C), paramagnetic susceptibility (χ_P), estimated percentage of Co ions ferromagnetically coupled (n_{FM}), and estimated magnetic moment per Co^{2+} ion (μ).

x_E	M_S (emu/g)	H_C (Oe)	$\chi_P \times 10^{-6}$ (emu/gOe)	n_{FM} (%)	μ (μ_B)
0.020(4)	0.0018(1)	40(3)	2.35(1)	-	-
0.078(2)	7.9(2)	395(3)	6(1)	35(7)	4(1)

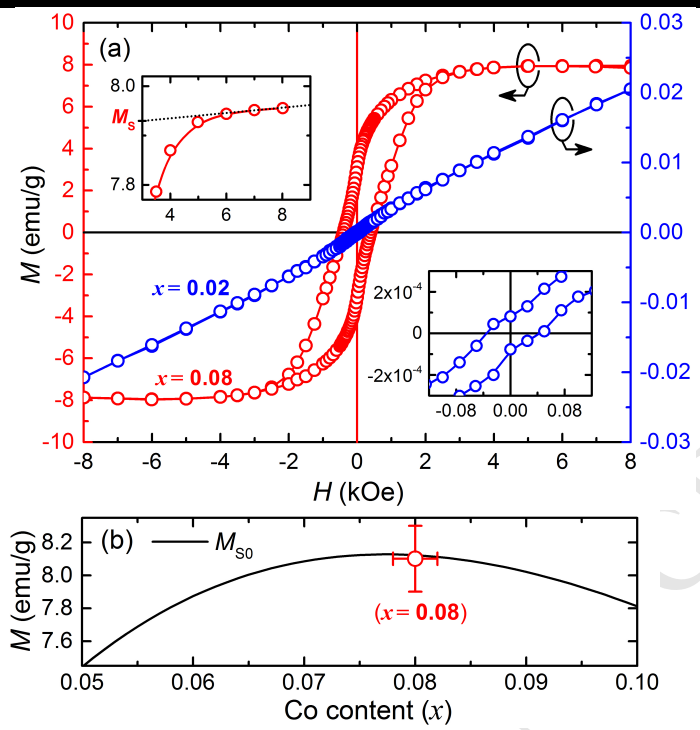

Fig. 4. (a) $M(H)$ curves obtained at room temperature for the nanoparticulate Co-doped ZnO thin films. The lower-right inset show the coercive field around 0.08 kOe for the thin film with x = 0.02, and the upper-left inset show the linear increase of M at high H for the thin film with x = 0.08. M is expressed in terms of emu/g considering the ZnO density of 5.61 g/cm^3. (b) M_{S0} for the fraction of Co ions in the single state as a function of the total Co concentration and the observed M_S for the sample with x = 0.08.

The magnetic moment per Co ion (μ) for the thin film with x = 0.08 can be derived from the following calculation (due to the magnitude of the errors, the same calculation for the thin film with x = 0.02 returned no significant results). Since we have a coexistence of paramagnetic (P) and a ferromagnetic (FM) phase, the total magnetization of the system is expressed in terms of its components as $M_T = M_P + M_{FM}$, where $M_P = \chi_P H$. At high temperatures the paramagnetic susceptibility can be written as $\chi_P = N_P \mu_P^2 / 3k_B T$, where N_P is the number of Co ions in the paramagnetic state, and k_B is the Boltzmann constant. The value for the μ_P is assumed to be that measured for the Co^{2+} high spin state, 4.8 μ_B [52], and the temperature (T) was 300 K. On the other hand, the saturation magnetization of the ferromagnetic component is $M_{FM} = \mu_{FM} N_{FM}$, where N_{FM} is the

number of Co ions ferromagnetically coupled. The total number of Co ions is assumed to be equal to the sum of N_{FM} and N_P. From the obtained χ_P, the N_P is extracted and the N_{FM} is calculated. With N_{FM} and M_{FM} in hands, the estimative of μ_{FM} is simply calculated. The Table 1 also present the others magnetic parameters involved in the calculus. The obtained average magnetic moment per Co ion of 4 ± 1 μ_B cannot be addressed to metallic Co cluster or possible known ferromagnetic phases [53-55], what lead us to definitively conclude that the observed ferromagnetic phase is an intrinsic property of the Co-doped ZnO thin films.

For DMSs and DMOs, considering a random distribution of the dopants over the host matrix, there will be always, besides the isolated dopants at the paramagnetic state (the singles), the formation of dopant clusters (pairs, triplets, quartets and so on) that will couple together, in a general way, antiferromagnetically, leading to the usual observed paramagnetic phase [56]. Therefore, only the uncompensated spins in the different magnetic clusters could be, in principle, ferromagnetically coupled. As listed in Tab. 1, the thin film with x = 0.08 has ~35% of the Co ions in the ferromagnetic state. At the doped concentration of x = 0.08, the probability for "singles" (isolated dopant ions – paramagnetic case) is exactly 36.8%. In principle the observed magnetization can be attributed to the ferromagnetic coupling between solely to the Co ions in the ZnO host matrix that is found in the single state. To illustrate the case, Fig. 4(b) presents the theoretical saturation magnetization (M_{S0}) as a function of the total Co concentration and the observed saturation magnetization for the sample with x = 0.08. In the calculus of the M_{S0} it was considered only the fraction of the Co ions in the single state and the magnetic moment per Co ion as given in Table 1. The full expression for the fraction of the Co ions in the single state can be found in Refs. [57, 58]. As can be seen, the concordance between M_{S0} value and the M_S experimentally measured are evident. Therefore, the consideration about the observed ferromagnetism be localized in fractions of the volume of the samples (interfaces, grain boundaries and etc.), as in the CTF model and in the Straumal proposition, can be, discharged, as the

"singles" are assumed to be randomly distributed over the entire volume of the samples. In fact, even considering the Straumal proposal, both our samples present an average grain size over the threshold value of 33 nm and, consequently, this model cannot explain the RTFM for the thin films with x = 0.08. Besides, the carrier-mediated mechanism also cannot explain the observed RTFM, since the Co^{2+} insertion into the Zn^{2+} sites of the ZnO matrix cannot lead to changes into the carrier concentration [59].

The nature of the observed RTFM can be fully analyzed under the scope of the BMP model. The kernel point in the theory is the hybridization between the magnetic dopant and the defect so carriers at the Fermi level are partially delocalized onto the magnetic dopants. For the particular case of the Co-doped ZnO, the Co^{2+} ions can hybridize effectively with shallow-donor impurity bands in ZnO because the states related to the complex Co^{+} (Co^{2+} + e^{-}_{donor}) are also of shallow-donor character [60]. As we have shown, for the thin film with x = 0.08 we observe a low energy absorption tail at the absorption spectrum (Fig. 2(c)), corresponding to transition from de valence band to free states at an energy band just below the ZnO band edge. Besides, this low energy absorption tail is almost negligible for the thin film with x = 0.02, as compared to the absorption spectrum obtained for an undoped ZnO reference sample. This low energy absorption band can be direct ascribed to the Co^{+} band [47]. Therefore, we can conclude that the different observed magnetic response for both studied thin films reside mainly in the presence and the absence of the necessary shallow-donor defects for the thin film with x = 0.08 and x = 0.02, respectively.

Considering the question about the nature of the necessary shallow-donor defect. Several experimental reports argue that the RTFM in the TM-doped ZnO system, explained in terms of the BMP model, is associated to oxygen vacancies (V_O) [47, 61-63]. However, our results clearly do not indicate that. As presented before, the XPS data reveals for the thin film with x = 0.02 a density of V_O higher than that for the thin film with x = 0.08, and while the latter presents a robust RTFM, the former

presents only a very small magnetization. In fact, the defect state related to V_O in the wurtzite ZnO structure has a donor character, however it is a deep-donor state [64, 65]. Although states of deeper-donors can hybridize to magnetic dopants, their smaller Bohr radii would require relatively higher dopant and defect concentrations to achieve a necessary spatial overlapping, however at such short-range antiferromagnetic superexchange interactions would take place. Instead, the most promising shallow-donor defect in the ZnO structure is the zinc interstitials (Zn_i) [65, 66]. From the experimental point of view, there are a growing number of reports in the literature giving clear evidences of the relation between the observed RTFM and defects at the zinc sites [67-70]. Even considering different systems, like undoped ZnO [71-73], Co-doped TiO_2 [74] and Cu-doped CeO_2 [75], the direction turns now to defects at cation sites as the responsible ones to promoting the desired ferromagnetic order.

4. CONCLUSIONS

We have presented a structural and magnetic analyzis of nanostructured Co-doped ZnO thin films prepared via EB-PVD. All the results obtained in structural characterization by the conjugation of different techniques confirms that the Co ions in the thin films stays in character substitutional to the Zn ions in the wurtzite ZnO structure with oxidation state 2+. There was no indication of metallic Co or other secondary foreign phases. Magnetization measurements reveal a robust ferromagnetism at room temperature for the sample with higher Co concentration (x = 0.08). The estimative for the magnetic moment per Co^{2+} ion was of ~4 μB, indicating that the obtained ferromagnetic order was an intrinsic property of the system. By the relative percentage of the number of the ferromagnetically coupled Co^{2+} ions, ~35%, it was possible to infer that the ferromagnetism were located around the entire volume of the thin films, and not only in the interface, or in the grain boundaries. Which lead us to evoke the BMP model to explain the obtained magnetic data. The hybridization of a shallow-donor impurity band with states of the Co^{2+} ions were observed at the UV-VIS analysis. XPS results also

show no correlation between the ferromagnetism and the densities of oxygen vacancies. Therefore, the zinc interstitials are the most promising defect of shallow-donor character necessary in the context of the BMP model.

ACKNOWLEDGEMENTS

Support from agencies FAPEMIG (APQ-02486-14; APQ-00273-14), CNPq (448723/2014-0; 308162/2015-3, 470069/2013-9), FAPESP (2013/07909-4), FINEP (Ref. 134/08) and CAPES (PNPD-2011) are gratefully acknowledged. We also thank CNPq (WAAM, MIBB and ACD) and CAPES (NCM, AOZ) for research fellowships. The authors also acknowledge Prof. Dr. F. Iikawa and Profa. Dra. M. J. S. Brasil of the Universidade de Campinas (UNICAMP) for the Raman measurements.

REFERENCES

1. Baibich, M.N., et al., *GIANT MAGNETORESISTANCE OF (001)FE/(001) CR MAGNETIC SUPERLATTICES.* Physical Review Letters, 1988. **61**(21): p. 2472-2475.
2. Binasch, G., et al., *ENHANCED MAGNETORESISTANCE IN LAYERED MAGNETIC-STRUCTURES WITH ANTIFERROMAGNETIC INTERLAYER EXCHANGE.* Physical Review B, 1989. **39**(7): p. 4828-4830.
3. Dieny, B., et al., *GIANT MAGNETORESISTANCE IN SOFT FERROMAGNETIC MULTILAYERS.* Physical Review B, 1991. **43**(1): p. 1297-1300.
4. Johnson, M., *Theory of spin-dependent transport in ferromagnet-semiconductor heterostructures.* Physical Review B, 1998. **58**(15): p. 9635-9638.
5. Knobel, M., et al., *Magnetic and magnetotransport properties of Co thin films on Si.* Physica Status Solidi a-Applied Research, 2001. **187**(1): p. 177-188.
6. Schmidt, G., et al., *Fundamental obstacle for electrical spin injection from a ferromagnetic metal into a diffusive semiconductor.* Phys. Rev. B, 2000. **62**(8): p. R4790-R4793.
7. Tang, H.X., et al., *Ballistic spin transport in a two-dimensional electron gas.* Physical Review B, 2000. **61**(7): p. 4437-4440.
8. Rashba, E.I., *Theory of electrical spin injection: Tunnel contacts as a solution of the conductivity mismatch problem.* Physical Review B, 2000. **62**(24): p. R16267-R16270.

9. Jiang, X., et al., *Highly spin-polarized room-temperature tunnel injector for semiconductor spintronics using MgO(100).* Physical Review Letters, 2005. **94**(5).
10. Ohno, H., *Making nonmagnetic semiconductors ferromagnetic.* Science, 1998. **281**(5379): p. 951-956.
11. Fukuma, Y., et al., *Carrier-induced ferromagnetism in Ge0.92Mn0.08Te epilayers with a Curie temperature up to 190 K.* Applied Physics Letters, 2008. **93**(25).
12. Wang, M., et al., *Achieving high Curie temperature in (Ga, Mn)As.* Applied Physics Letters, 2008. **93**(13).
13. Dietl, T., et al., *Zener model description of ferromagnetism in zinc-blende magnetic semiconductors.* Science, 2000. **287**(5455): p. 1019-1022.
14. Venkatesan, M., et al., *Anisotropic ferromagnetism in substituted zinc oxide.* Physical Review Letters, 2004. **93**(17).
15. Chambers, S.A., et al., *Epitaxial growth and properties of ferromagnetic co-doped TiO2 anatase.* Applied Physics Letters, 2001. **79**(21): p. 3467-3469.
16. Punnoose, A., et al., *Room-temperature ferromagnetism in chemically synthesized Sn1-xCoxO2 powders.* Applied Physics Letters, 2004. **85**(9): p. 1559-1561.
17. Ogale, S.B., *Dilute Doping, Defects, and Ferromagnetism in Metal Oxide Systems.* Advanced Materials, 2010. **22**(29): p. 3125-3155.
18. Dutta, S., et al., *Role of defects in tailoring structural, electrical and optical properties of ZnO.* Progress in Materials Science, 2009. **54**(1): p. 89-136.
19. Huang, F., et al., *Research progress in ZnO single-crystal: growth, scientific understanding, and device applications.* Chinese Science Bulletin, 2014. **59**(12): p. 1235-1250.
20. Coey, J.M.D., M. Venkatesan, and C.B. Fitzgerald, *Donor impurity band exchange in dilute ferromagnetic oxides.* Nature Materials, 2005. **4**(2): p. 173-179.
21. Coey, J.M.D., et al., *Ferromagnetism in Fe-doped SnO2 thin films.* Applied Physics Letters, 2004. **84**(8): p. 1332-1334.
22. Coey, J.M.D., et al., *Charge-transfer ferromagnetism in oxide nanoparticles.* Journal of Physics D-Applied Physics, 2008. **41**(13): p. 134012.
23. de Godoy, M.P.F., et al., *Evidence of defect-mediated magnetic coupling on hydrogenated Co-doped ZnO.* Journal of Alloys and Compounds, 2013. **555**: p. 315-319.
24. Straumal, B.B., et al., *Magnetization study of nanograined pure and Mn-doped ZnO films: Formation of a ferromagnetic grain-boundary foam.* Physical Review B, 2009. **79**(20).
25. Tietze, T., et al., *Interfacial dominated ferromagnetism in nanograined ZnO: a mu SR and DFT study.* Scientific Reports, 2015. **5**.
26. de Carvalho, H.B., et al., *Absence of ferromagnetic order in high quality bulk Co-doped ZnO samples.* Journal of Applied Physics, 2010. **108**(3).
27. De Vicente, F.S., E.A.A. Rubo, and M.S. Li, *Construction of an evaporation system for film deposition via resistive and electron beam sources.* Revista Brasileira de Aplicações de Vácuo, 2004. **23**(1): p. 11-16.
28. Singh, S. and M. Rao, *Optical and electrical resistivity studies of isovalent and aliovalent 3d transition metal ion doped ZnO.* Physical Review B, 2009. **80**(4).

29. Calleja, J.M. and M. Cardona, *Resonant Raman-Scattering in Zno.* Phys. Rev. B, 1977. **16**(8): p. 3753-3761.
30. Cusco, R., et al., *Temperature dependence of raman scattering in ZnO.* Physical Review B, 2007. **75**(16).
31. Damen, T.C., S.P.S. Porto, and B. Tell, *RAMAN EFFECT IN ZINC OXIDE.* Physical Review, 1966. **142**(2): p. 570-&.
32. Mesquita, A., et al., *Dynamics of the incorporation of Co into the wurtzite ZnO matrix and its magnetic properties.* Journal of Alloys and Compounds, 2015. **637**: p. 407-417.
33. Wang, Z.H., et al., *Raman spectra and room-temperature ferromagnetism of hydrogenated Zn0.95Mn0.05O nanopowders.* Journal of Applied Physics, 2009. **105**(12).
34. Wang, X., et al., *Structural evidence of secondary phase segregation from the Raman vibrational modes in Zn1-xCoxO (0 < x < 0.6).* Appl. Phys. Lett., 2007. **91**(3): p. 031908.
35. Phan, T.L., et al., *Enhancement of multiple-phonon resonant Raman scattering in Co-doped ZnO nanorods.* Applied Physics Letters, 2008. **93**(8).
36. Wang, J.B., et al., *Raman scattering and high temperature ferromagnetism of Mn-doped ZnO nanoparticles.* Applied Physics Letters, 2006. **88**(25).
37. Cheng, B.C., et al., *The vibrational properties of one-dimensional ZnO : Ce nanostructures.* Applied Physics Letters, 2004. **84**(3): p. 416-418.
38. Bundesmann, C., et al., *Raman scattering in ZnO thin films doped with Fe, Sb, Al, Ga, and Li.* Applied Physics Letters, 2003. **83**(10): p. 1974-1976.
39. Callender, R.H., et al., *DISPERSION OF RAMAN CROSS-SECTION IN CDS AND ZNO OVER A WIDE ENERGY RANGE.* Phys. Rev. B, 1973. **7**(8): p. 3788-3798.
40. Reuss, F., et al., *Optical investigations on the annealing behavior of gallium- and nitrogen-implanted ZnO.* Journal of Applied Physics, 2004. **95**(7): p. 3385-3390.
41. Limpert, E., W. Stahel, and M. Abbt, *Log-normal distributions across the sciences: Keys and clues.* Bioscience, 2001. **51**(5): p. 341-352.
42. Weakliem, H.A., *OPTICAL SPECTRA OF NI2+, CO2+, AND CU2+ IN TETRAHEDRAL SITES IN CRYSTALS.* Journal of Chemical Physics, 1962. **36**(8): p. 2117-&.
43. Koidl, P., *OPTICAL-ABSORPTION OF CO2+ IN ZNO.* Physical Review B, 1977. **15**(5): p. 2493-2499.
44. Lee, J.D., *Concise Inorganic Chemistry*. 5th ed. 1996, London: ELBS with Chapman and Hall.
45. Shannon, R., *Revised effective ionic radii and systematic studies of interatomic distances in halides and chalcogenides.* Acta Crystallographica Section A, 1976. **32**(5): p. 751-767.
46. Wagner, C.D., et al., *Handbook of X-ray Photoelectron Spectroscopy*. 1978 Minnesota: Perkin-Elmer Corporation.
47. Ivill, M., et al., *Structure and magnetism of cobalt-doped ZnO thin films.* New Journal of Physics, 2008. **10**.
48. Islam, M.N., et al., *XPS and X-ray diffraction studies of aluminum-doped zinc oxide transparent conducting films.* Thin Solid Films, 1996. **280**(1-2): p. 20-25.

49. Tyuliev, G. and S. Angelov, *THE NATURE OF EXCESS OXYGEN IN CO3O4+EPSILON.* Applied Surface Science, 1988. **32**(4): p. 381-391.
50. Fan, J.C.C. and J.B. Goodenough, *X-RAY PHOTOEMISSION SPECTROSCOPY STUDIES OF SN-DOPED INDIUM-OXIDE FILMS.* Journal of Applied Physics, 1977. **48**(8): p. 3524-3531.
51. Wei, X.Q., et al., *Blue luminescent centers and microstructural evaluation by XPS and Raman in ZnO thin films annealed in vacuum, N-2 and O-2.* Physica B-Condensed Matter, 2007. **388**(1-2): p. 145-152.
52. Kittel, C., *Introduction to solid state physics*. 7th ed. ed. 1996, New York ; Chichester: Wiley.
53. Bucher, J.P., D.C. Douglass, and L.A. Bloomfield, *MAGNETIC-PROPERTIES OF FREE COBALT CLUSTERS.* Physical Review Letters, 1991. **66**(23): p. 3052-3055.
54. Fan, H.J., C.W. Liu, and M.S. Liao, *Geometry, electronic structure and magnetism of small Co-n (n=2-8) clusters.* Chemical Physics Letters, 1997. **273**(5-6): p. 353-359.
55. Goodenough, J.B., *Magnetism and the Chemical Bond*. 1963, New York Interscience.
56. Shapira, Y. and V. Bindilatti, *Magnetization-step studies of antiferromagnetic clusters and single ions: Exchange, anisotropy, and statistics.* Journal of Applied Physics, 2002. **92**(8): p. 4155-4185.
57. Shapira, Y., et al., *TECHNICAL SATURATION AND MAGNETIZATION STEPS IN DILUTED MAGNETIC SEMICONDUCTORS - PREDICTIONS AND OBSERVATIONS.* Physical Review B, 1984. **30**(7): p. 4021-4023.
58. Liu, M.T., et al., *Magnetization steps of spin quartets.* Physical Review B, 1996. **54**(9): p. 6457-6464.
59. Zhan, Z.B., et al., *Strategy for Preparing Al-Doped ZnO Thin Film with High Mobility and High Stability.* Crystal Growth & Design, 2011. **11**(1): p. 21-25.
60. Kittilstved, K.R., W.K. Liu, and D.R. Gamelin, *Electronic structure origins of polarity-dependent high-T-C ferromagnetismin oxide-diluted magnetic semiconductors.* Nature Materials, 2006. **5**(4): p. 291-297.
61. Ramachandran, S., J. Narayan, and J.T. Prater, *Effect of oxygen annealing on Mn doped ZnO diluted magnetic semiconductors.* Applied Physics Letters, 2006. **88**(24).
62. Hsu, H.S., et al., *Evidence of oxygen vacancy enhanced room-temperature ferromagnetism in Co-doped ZnO.* Applied Physics Letters, 2006. **88**(24).
63. Tietze, T., et al., *XMCD studies on Co and Li doped ZnO magnetic semiconductors.* New Journal of Physics, 2008. **10**.
64. Janotti, A. and C.G. Van de Walle, *Native point defects in ZnO.* Physical Review B, 2007. **76**(16).
65. Xu, P., et al., *The electronic structure and spectral properties of ZnO and its defects.* Nuclear Instruments & Methods in Physics Research Section B-Beam Interactions With Materials and Atoms, 2003. **199**: p. 286-290.
66. Look, D.C., J.W. Hemsky, and J.R. Sizelove, *Residual native shallow donor in ZnO.* Physical Review Letters, 1999. **82**(12): p. 2552-2555.
67. de Almeida, V.M., et al., *Room temperature ferromagnetism promoted by defects at zinc sites in Mn-doped ZnO.* Journal of Alloys and Compounds, 2016. **655**: p. 406-414.
68. Zhang, H.Y., et al., *Room temperature ferromagnetic Zn0.98Co0.02O powders with improved visible-light photocatalysis.* Rsc Advances, 2016. **6**(8): p. 6761-6767.
69. Shah, L.R., et al., *Effect of Zn interstitials on the magnetic and transport properties of bulk Co-doped ZnO.* Journal of Physics D-Applied Physics, 2010. **43**(3).

70. Khare, N., et al., *Defect-induced ferromagnetism in co-doped ZnO.* Advanced Materials, 2006. **18**(11): p. 1449-+.

71. Yi, J.B., et al., *Ferromagnetism in Dilute Magnetic Semiconductors through Defect Engineering: Li-Doped ZnO.* Physical Review Letters, 2010. **104**(13): p. 137201.

72. Ghose, S., et al., *Role of Zn-interstitial defect states on d(0) ferromagnetism of mechanically milled ZnO nanoparticles.* Rsc Advances, 2015. **5**(121): p. 99766-99774.

73. Aljawf, R.N.R., F. and S. Kumar, *Defects/vacancies engineering and ferromagnetic behavior in pure ZnO and ZnO doped with Co nanoparticles.* Materials Research Bulletin, 2016. **83**: p. 8.

74. de Souza, T.E., et al., *Structural and Magnetic Properties of Dilute Magnetic Oxide Based on Nanostructured Co-Doped Anatase TiO2 (Ti1-xCoxO2-delta).* Journal of Physical Chemistry C, 2013. **117**(25): p. 13252-13260.

75. Bernardi, M.I.B., et al., *The role of oxygen vacancies and their location in the magnetic properties of Ce1-xCuxO2-delta nanorods.* Physical Chemistry Chemical Physics, 2015. **17**(5): p. 3072-3080.

MINISTÉRIO DA EDUCAÇÃO
Universidade Federal de Alfenas . Unifal-MG
Rua Gabriel Monteiro da Silva, 700 . Alfenas/MG . CEP 37130-000
Fone: (35) 3299-1000 . Fax: (35) 3299-1063
INSTITUTO DE CIÊNCIAS EXATAS
Fone/Fax (35) 3299-1384

Highlights

Title: On the nature of the room temperature ferromagnetism in nanoparticulate Co-doped ZnO thin films prepared by EB-PVD

Authors: Niko Churata Mamani, Rafael Tomaz da Silva, Angela Ortiz de Zevallos, Alexandre Alberto Chaves Cotta, Waldemar Augusto de Almeida Macedo, Máximo Siu Li, Maria Inês Basso Bernardi, Antonio Carlos Doriguetto and Hugo Bonette de Carvalho

Corresponding Author:
Dr. Hugo Bonette de Carvalho
Universidade Federal de Alfenas – UNIFAL-MG
Rua Gabriel Monteiro da Silva, 700
Centro - Alfenas/MG
CEP: 37130-000
e-mail: bonette@gmail.com / bonette@unifal-mg.edu.br

- Co-doped ZnO ($Zn_{1-x}Co_xO$, x = 0.02 and 0.08) films were prepared by EB-PVD method.
- Structural analyses detects a lower density of V_O for sample with x = 0.08.
- Optical results show the existence of a defect sub-band close to conduction band.
- Magnetic data reveal a huge M_S for the film with x = 0.08, not correlated to V_O.
- Magnetic properties are analyzed in the scope of BMP theory related to Zn_i defects.